THE JOURNAL OF PHYSICAL CHEMISTRY Letters

Letter

pubs.acs.org/JPCL

Sub-Nanometer-Resolution Elemental Mapping of "Pt_3Co" Nanoparticle Catalyst Degradation in Proton-Exchange Membrane Fuel Cells

Christopher E. Carlton,[†] Shuo Chen,[†] Paulo J. Ferreira,[‡] Lawrence F. Allard,[§] and Yang Shao-Horn*,[†]

[†]Department of Mechanical Engineering and Department of Materials Science and Engineering, Massachusetts Institute of Technology, Cambridge, Massachusetts 02139, United States

[‡]Materials Science and Engineering Program, University of Texas at Austin, Austin, Texas 78712, United States

[§]Materials Science and Technology Division, Oak Ridge National Laboratory, Oak Ridge, Tennessee 37831, United States

Supporting Information

ABSTRACT: The efficiency of proton exchange membrane fuel cells (PEMFCs) is limited largely by sluggish oxygen reduction reaction (ORR) kinetics, even when promoted by Pt-based alloy nanoparticles (NPs). Acid-leached Pt alloys such as "Pt_3Co" have shown considerably higher specific (2−5 times) and mass (2 to 3 times) ORR activity than Pt NPs. However, the specific activity enhancement of "Pt_3Co" NPs decreases during PEMFC operation, which has been attributed to the formation of a Pt-enriched shell near the NP surfaces. In this study, we report direct evidence of surface Pt and Co compositional changes in acid-treated "Pt_3Co" NPs after PEMFC voltage cycling using energy-dispersive spectroscopy mapping in an aberration-corrected scanning transmission electron microscope with subnanometer resolution. Acid-treated "Pt_3Co" NPs were found to have Pt-enriched shells of ∼0.5 nm, whereas the Pt-enriched-shell became thicker (∼1−6 nm) after PEMFC voltage cycling, where greater shell thicknesses were associated with larger "Pt_3Co" NPs.

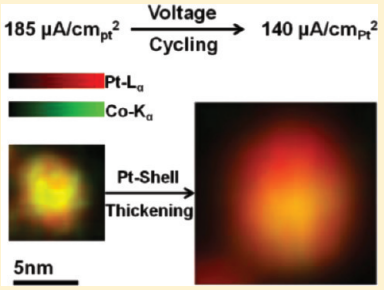

SECTION: Surfaces, Interfaces, Catalysis

Proton exchange membrane fuel cells (PEMFCs) are promising energy conversion devices for automotive applications, but the slow oxygen reduction reaction (ORR) kinetics catalyzed by Pt-based catalysts limits their efficiency and cost.[1] Studies have shown that Pt-alloy surfaces can weaken binding of oxygenated species,[2] and enhance intrinsic ORR activities relative to bulk Pt.[2−8] For example, acid leaching of bulk Pt alloys can result in Pt enrichment in the near-surface regions causing intrinsic ORR activity two to three times higher than Pt.[4,6] Recently, aberration-corrected scanning transmission electron microscopy (STEM) imaging[9,10] of acid-leached Pt-alloy nanoparticles (NPs) has provided evidence of the presence of skeleton Pt-enriched surface regions similar to those proposed for bulk Pt surfaces[4,6] (Scheme 1a). However, the specific activities of Pt-alloy NPs decrease over time during exposure to fuel cell operating conditions, especially under voltage cycling.[11−13] It is hypothesized that the activity loss of Pt-alloy NPs results from thickening of Pt shells (Scheme 1a) during PEMFC voltage cycling, which might be associated with reduction and deposition of Pt^{z+} ions dissolved from small particles on the surface of large particles in an Oswald ripening-like process.[14,15] Therefore, it is of great importance to understand how the surface composition of Pt-alloy NPs changes during voltage cycling.

In this study, we employ aberration-corrected STEM energy-dispersive spectroscopy (EDS) mapping with a spatial resolution of ∼0.5 nm to study the surface compositional changes of "Pt_3Co" NPs in a PEMFC membrane electrode assembly (MEA) cathode before and after voltage cycling. Although recent aberration-corrected STEM spectroscopy studies have revealed surface compositions of as-synthesized Pt-alloy NPs,[9,10,16−21] understanding of alloy NP stability is very limited. Our recent conventional STEM studies[14] have used EDS analysis of Pt and Co from discrete spots across individual "Pt_3Co" NPs to show the growth of Pt-enriched surface regions and the development of core/shell NPs upon PEMFC potential cycling. However, the low spatial resolution of ∼2.5 nm only allows for the analysis of "Pt_3Co" NPs of ∼10 nm or greater and fails to resolve the Pt shell that is expected to have an average thickness of ∼1.5 nm.[14] Here we report EDS Pt and Co maps of individual NPs, which clearly resolve skeleton Pt-enriched regions of "Pt_3Co" NPs (obtained from acid leaching) in the pristine MEA cathode, and the formation of nearly pure Pt shells greater than 1 nm thick on the NP surface in the voltage-cycled MEA cathode.

Aberration-corrected STEM high-angle annular dark-field (HAADF) imaging of pristine and cycled MEA cathode cross sections, having high sensitivity to mass contrast, shows Pt loss

Received: December 6, 2011
Accepted: December 29, 2011
Published: December 29, 2011

   dx.doi.org/10.1021/jz2016022 | J. Phys. Chem.Lett. 2012, 3, 161−166

Scheme 1. Proposed Changes in "Pt_3Co" NPs during PEMFC Potential Cycling by Chen et al.[14] [a]

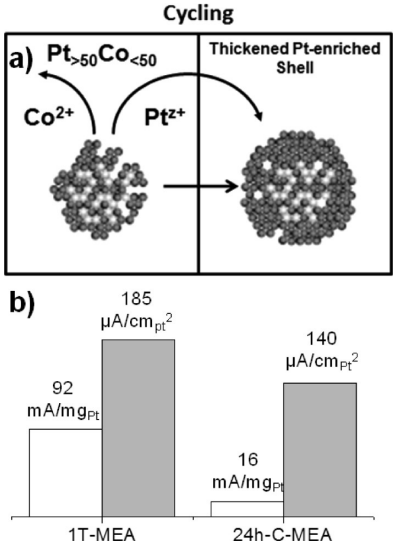

[a]Top panel (a) shows the proposed changes in acid-leached "Pt_3Co" NPs during PEMFC potential cycling while the bottom panel (b) shows the loss of specific activity and mass activity in"Pt_3Co" NPs before and after PEMFC potential cycling.[14] 1T-MEA refers to the pristine MEA PEMFC-tested for one time, and 24h-C-MEA refers to the 24 h cycled MEA.

from the cathode and "Pt_3Co" size changes during voltage cycling. HAADF imaging of MEA cathode cross sections at low magnifications clearly reveals the distribution of "Pt_3Co" NPs (shown as bright spots). Similar to previous work,[14] "Pt_3Co" NPs were dispersed homogeneously across the entire pristine cathode cross-section (Figure 1a and Figure S1 of the Supporting Information). In contrast, the density of "Pt_3Co" NPs in the cycled cathode was found to decrease from the interface between diffusion media (DM) and cathode to the interface between cathode and membrane (Figure 1b and Figure S2 of the Supporting Information), and a band of Pt NPs was noted in the membrane near the interface between cathode and membrane. The decreased density of "Pt_3Co" NPs and the formation of the pure Pt band in the membrane of the cycled MEA can be explained by dissolution of Pt and Co ions from small particles and the reduction of dissolved Pt^{Z+} ions (the reduction of Co ions by H_2 is thermodynamically unfavorable[14]) by H_2 permeating through the membrane from the anode side,[15,22–24] respectively. Quantification of the HAADF intensity (Figure S3 of the Supporting Information) shows that the average HAADF intensity of regions of the cycled cathode decreased considerably from the DM/cathode interface to the cathode/membrane interface, which suggests that the majority of the Pt mass lost from the cathode occurred in the cathode regions near the membrane.[14]

HAADF imaging of pristine and cycled MEA cathode cross sections at high magnifications showed two morphologies for "Pt_3Co" NPs: majority and minority particles, which most likely resulted from acid leaching of "$Pt_{>0.5}Co_{<0.5}$" and "$Pt_{<0.5}Co_{>0.5}$" NPs during catalyst synthesis, respectively.[14] The majority dense particles (pristine: ~4 nm and cycled: ~8 nm), which are characterized by relatively homogeneous HAADF intensities, comprise ~90% of observed particles (Figures S4a-b and S5a-b of the Supporting Information) and are largely responsible for the specific activity of the MEA cathode. The growth of these

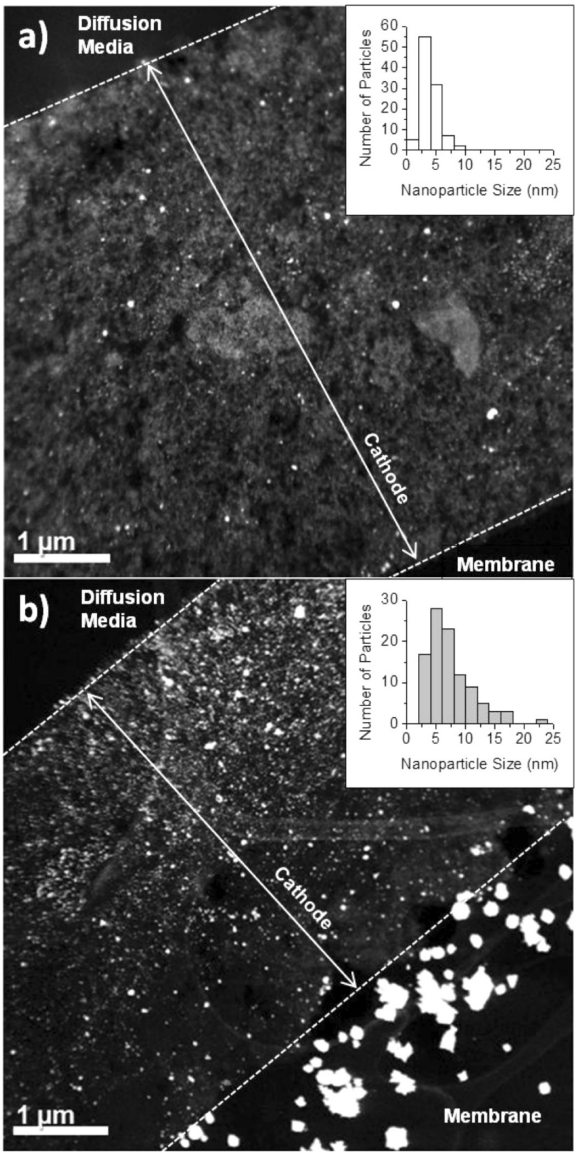

Figure 1. Aberration-corrected, HAADF STEM images of the entire "Pt_3Co" cathode cross-section from the pristine (a) and cycled (b) MEAs. Particle size distributions of "Pt_3Co" NPs are shown in the insets.

particles in the cycled MEA cathode (Figure 1a,b inserts) can be explained by dissolution of smaller NPs and growth of larger NPs. The minority particle morphology consists of percolated particles with sizes ranging from ~10 to ~50 nm, which display significant intensity variations in the HAADF images (Figures S4c-d and S5c-d of the Supporting Information).

Aberration-corrected STEM EDS mapping of Pt and Co of individual majority "Pt_3Co" NPs in the pristine MEA shows direct evidence of skeleton Pt enrichment in the near-surface regions, as shown in Figure 2 and Figure S6 of the Supporting Information. Combined Pt L_α (red) and Co K_α (green) X-ray maps of two "Pt_3Co" NPs with diameters of ~5 nm show that some surface regions (skeleton) were enriched with Pt relative to the particle core, as shown by Figure 2a,b. Although these two "Pt_3Co" NPs had comparable average Pt and Co atomic percentages (Pt 77% in Figure 2a and Pt 76% in Figure 2b), in agreement with NPs of similar sizes in previous work,[14] the distributions of Pt and Co within these particles were

dx.doi.org/10.1021/jz2016022 | J. Phys. Chem.Lett. 2012, 3, 161–166

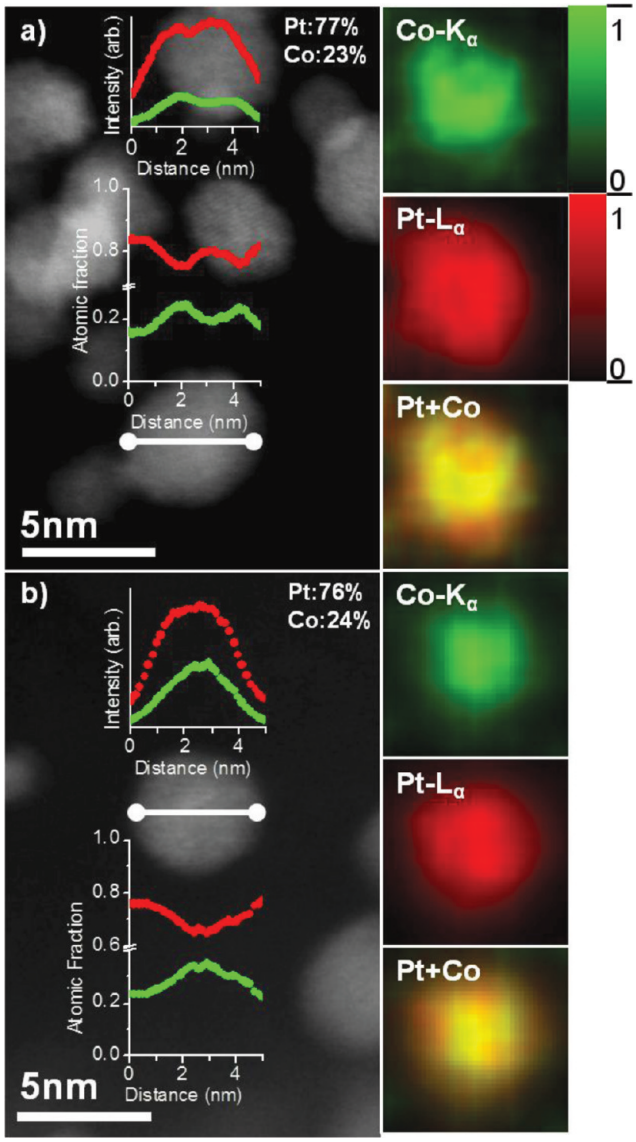

Figure 2. (a,b) Aberration-corrected HAADF STEM images (on the left) and EDS Pt and Co maps (on the right) of two acid-leached "Pt_3Co" NPs in the pristine MEA. Sensitivity-factor-corrected EDS intensity profiles that were taken along the white line drawn in the HAADF images and the corresponding composition profiles produced using the Cliff–Lorimer equation[26] are shown as insets.

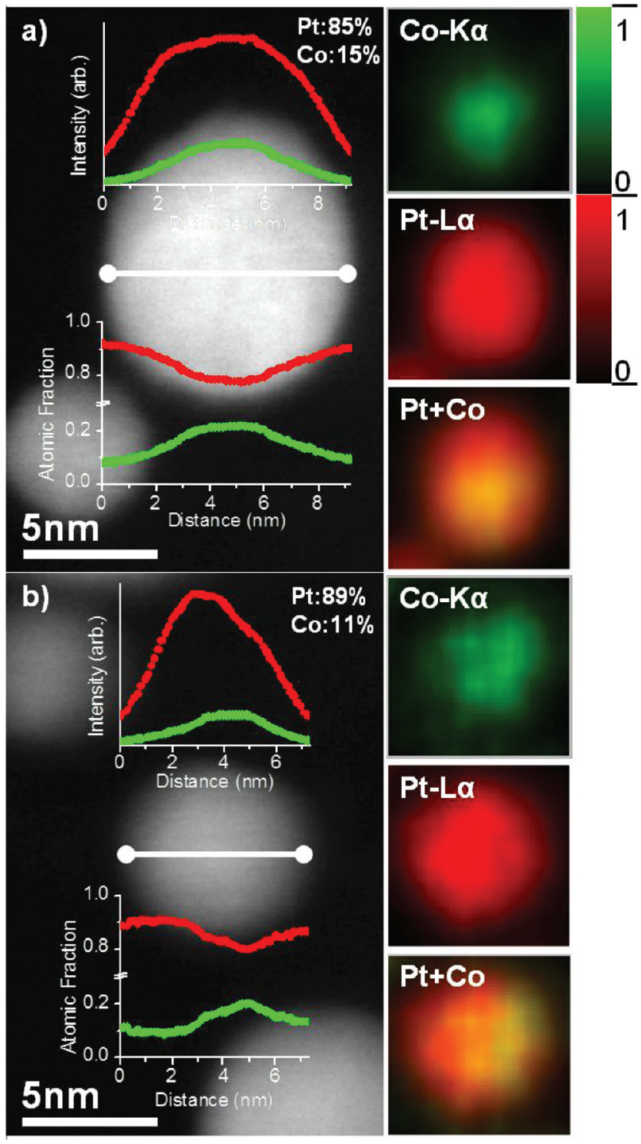

Figure 3. (a,b) Aberration-corrected STEM HAADF images and Pt and Co EDS maps of two "Pt_3Co" NPs, with sizes between 5 and 10 nm, collected from the cycled MEA. Sensitivity-factor-corrected EDS intensity profiles that were taken along the white line drawn in the HAADF images and the corresponding composition profiles produced using the Cliff–Lorimer equation are shown as insets.

considerably different. The sensitivity-factor-corrected Pt and Co intensity profiles along the marked lines across the two NPs in Figure 2a,b further support surface Pt enrichment, and the compositional profiles estimated from the intensity line profiles show that the Pt-enriched surface regions had thicknesses of ~0.5 nm with higher Pt atomic concentrations of ~80–85%, whereas the core of these two particles had lower Pt atomic concentrations of ~65%. These results are in agreement with recent electron energy loss spectroscopy (EELS) work,[25] which also showed that acid-treated "Pt_3Co" NPs possessed ~0.6 nm thin Pt-enriched shells.

Aberration-corrected STEM EDS mapping of Pt and Co in individual majority "Pt_3Co" NPs in the cycled MEA showed direct evidence of the growth of surface Pt-enriched shells to 1–6 nm. Combined Pt L_α (green) and Co K_α (red) X-ray maps of two "Pt_3Co" NPs, with sizes between 5 and 10 nm, revealed that not only did they have higher Pt atomic percentages on average (Pt 85% in Figure 3a and Pt 89% in Figure 3b) but also thicker regions of Pt-enrichment near the surface (Figure 3a,b) than "Pt_3Co" NPs in the pristine MEA (Figure 2a,b). This is further supported by sensitivity-factor-corrected EDS intensity profiles of Pt L_α and Co K_α taken along the marked lines in Figure 3a,b. The compositional profiles estimated from the intensity line profiles show that the Pt-enriched shells formed on the surfaces of "Pt_3Co" NPs had thicknesses in the range from ~1 to ~2 nm, with Pt atomic concentrations of ~90%. In contrast, the core of these two particles had lower Pt atomic concentrations of ~75%. Comparison with the "Pt_3Co" NPs in the pristine MEA in Figure 2 suggests considerable surface Pt enrichment during voltage cycling, which can be attributed to Pt that dissolves from smaller NPs and is then reduced onto larger particles. Such processes have been used to explain the growth of Pt NPs in cycled MEA cathodes previously.[15,22−24] EDS mapping of "Pt_3Co" NPs larger than ~10 nm in the cycled

dx.doi.org/10.1021/jz2016022 | J. Phys. Chem.Lett. 2012, 3, 161–166

MEA provided further support to this hypothesis, where greater Pt-enriched shell thicknesses (~3−6 nm) (Figure S7 of the Supporting Information) were found in comparison with "Pt_3Co" NPs smaller than ~10 nm. This size-dependent Pt-shell growth is in agreement with the findings of recent EELS work.[25] The importance of MEA testing to the study of catalyst stability should be mentioned because the Pt-shell thickening/deposition of catalyst NPs would not have occurred in rotating disk electrode measurements, where a larger volume of acid is available for Pt dissolution than that of MEA cathode, and more Pt would have remained dissolved in acid.[24]

We propose that the development and thickening of the Pt-enriched shell on the surfaces of "Pt_3Co" NPs is primarily responsible for the specific activity loss of the PEMFC MEA cathode during voltage cycling based on the following arguments. First, as it is well known that Pt NPs larger than 5 nm have higher specific activity than smaller Pt NPs,[1,27,28] the reduced specific activity of "Pt_3Co" NPs in the cycled MEA cathode cannot be explained by their increased sizes relative to those in the pristine MEA cathode (Figure 1). Second, as the Pt-enriched shells formed during voltage-cycling were 1 nm and greater in thickness (corresponding to >4 monolayers), and considering that elements approximately four monolayers beneath the surface have negligible impact on the electronic structure of the surface layer,[29] the postulated catalytic enhancement from Co due to compressive strain[2,3,7,30−32] or ligand effects[4−7,33−35] should be significantly reduced for the voltage-cycled "Pt_3Co" NPs. Third, the specific activity of "Pt_3Co" NPs found in the cycled MEA is consistent with the specific activity of Pt NPs of comparable sizes.[1,3] Therefore, reducing Pt dissolution is key not only to limit Pt weight loss from the cathode (the formation of a Pt band in the membrane) but also to maintain the enhanced activity of Pt alloy NPs during PEMFC operation. Unlike recent EELS work,[25] we observed no evidence of coalescence or multicore NPs in the cycled MEA, which were reported to account for ~50% of the NPs larger than 6 nm in their cycled sample. This difference is not understood and requires further studies to develop durable catalysts for PEMFCs but might be attributed to different cycling conditions, Pt loadings, or carbon supports used. It is interesting to note that we observed some evidence of nonuniform Pt deposition on the surfaces of cycled "Pt_3Co" NPs, where Pt deposition may be influenced by the positions of nearby particles, and preferential deposition appears to occur on Pt particle surfaces close to nearby particles (Figure S7 of the Supporting Information). This can potentially lead to multicore particles, which cannot be explained solely by coalescence based on particle migration on carbon support.

Considerable compositional and morphological changes were noted for minority percolated NPs in the cycled MEA cathode (Figure 4). The formation of these percolated NPs is typically explained by dealloying[36,37] of Co in acid. Percolated particles in the pristine MEA had an average pore size of ~2 nm, which grew to ~7 nm in the cycled MEA, as shown in Figure 4. In addition, percolated NPs in the pristine MEA contained Pt atomic percentages of ~85%, whereas percolated NPs in the cycled MEA contained Pt atomic percentages of ~95%. The observation of larger pore sizes and higher Pt atomic percentages in percolated particles in the cycled MEA cathode than those in the pristine MEA cathode further reflects considerable Co and Pt dissolution from these particles during voltage cycling.

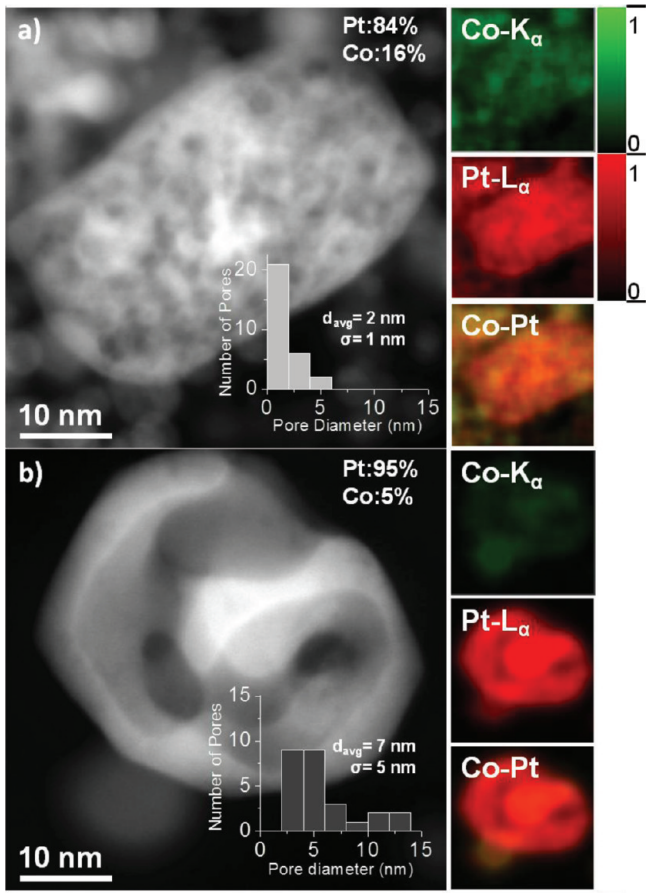

Figure 4. STEM HAADF images and Pt and Co EDS maps of percolated "Pt_3Co" particles from (a) the pristine and (b) cycled cathode. Pore size distributions of the pristine and cycled samples are shown in the insets, where the pores sizes were obtained from averaging their major and minor axes.

We demonstrate that aberration-corrected STEM-EDS imaging and associated EDS mapping is a powerful tool for determining the near-surface compositions of Pt-alloyed NPs. Compared with conventional STEM with spatial resolution of ~2.5 nm, which can show surface enrichment on NPs of 10 nm and greater, the aberration-corrected STEM EDS mapping results in this study reveal Pt and Co distributions in the near-surface regions of "Pt_3Co" NPs with subnanometer resolution. We show the formation of a Pt-enriched shell (90% Pt in atomic percentage) of ~1 to ~2 nm for "Pt_3Co" NPs smaller than ~10 nm, whereas thicker shells of ~3−6 nm are associated with NPs larger than ~10 nm in the cycled MEA cathode. The presence of Pt-enriched shells greater than ~1 nm on the surfaces of "Pt_3Co" NPs found in the cycled MEA is responsible for the specific activity loss of "Pt_3Co" NPs upon voltage cycling.

■ EXPERIMENTAL SECTION

Sample Preparation. "Pt_3Co" NPs supported on high-surface area carbon (Pt loading of 46% by weight) that was obtained from Tanaka KikinzokuKogyo (TKK) were used in the PEMFC cathode voltage-cycling studies. Voltage cycling of "Pt_3Co" MEAs was performed with fully humidified H_2 and dry N_2 at ambient pressures and a potential sweep between 650 and 1050 mV versus reversible hydrogen electrode and a rate of 100 mV/s for 24 h at 80 °C. The specific activity of "Pt_3Co" MEA

dx.doi.org/10.1021/jz2016022 | J. Phys. Chem.Lett. 2012, 3, 161−166

cathode, which was measured in a H_2/O_2 PEMFC at 80 °C after voltage cycling, was found to decrease from ~185 $\mu A/cm^2_{Pt}$ in the pristine to ~140 $\mu A/cm^2_{Pt}$ in the cycled MEA.[14] Detailed descriptions of MEA preparation, MEA testing, and STEM sample preparation can be found in the Supporting Information and in previous work.[14]

STEM Analysis. STEM analysis was conducted on a JEOL JEM 2200FS equipped with a CEOS aberration corrector (CEOS GmbH, Heidelberg, Ger) at the Oak Ridge National Laboratory High Temperature Materials Laboratory. HAADF images at 512 × 512 px were taken with a scan rate of 64 μs/px. Images and EDS maps were acquired in analytical mode (AMAG), with a probe size of 0.2 nm and a nominal beam current of 450 pA. The EDS signal was collected with a Bruker X-Flash silicon-drift detector and was processed using the Bruker Esprit software. EDS maps were collected for >10 min. The final resolution of the EDS maps was estimated to be ~0.5 nm. The EDS maps in Figures 2−4 were smoothed using a 7 × 7 px Kernel smoothing algorithm in the Bruker Esprit software, and the influence of smoothing can be found in Figure S6 of the Supporting Information. Details regarding EDS resolution, quantification, and processing are presented in the Supporting Information. The colors of the EDS maps were scaled universally to reflect the changes in the atomic concentrations of Pt and Co among different images. The color scale of "1" indicates the maximum EDS intensity of Pt or Co in the EDS map (corresponding to the maximum concentration) with the highest Pt or Co concentration in all of the manuscript and Supporting Information figures, respectively. For example, the maximum intensity of the Co K_α EDS map in Figure 1a was the highest Co concentration presented in this manuscript and Supporting Information, which was set to "1" on the color scale and was used to scale Co K_α intensities of all the other maps accordingly. This scaling allows for quick, accurate visual comparison of atomic concentrations among different images based on the Pt and Co EDS color scales.

■ ASSOCIATED CONTENT

Supporting Information

Experimental details regarding EDS processing and sample preparation, STEM HAADF images of the pristine and cycled MEA cathode, and STEM EDS analysis of percolated NPs. This material is available free of charge via the Internet at http://pubs.acs.org.

■ AUTHOR INFORMATION

Corresponding Author

*E-mail: shaohorn@mit.edu.

■ ACKNOWLEDGMENTS

This work was partially supported by the DOE Hydrogen Initiative program under award number DE-FG02-05ER15728 and the U.S. Department of Energy, Office of Energy Efficiency and Renewable Energy, Fuel Cell Technologies Program through Argonne National Laboratory under contract DE-AC02-06CH11357. The research made use of the Shared Experimental Facilities supported by the MRSEC Program of the National Science Foundation under award number DMR 08-019762. Microscopy work at Oak Ridge National Laboratory's High Temperature Materials Laboratory was sponsored by the U.S. Department of Energy, Office of Energy Efficiency and Renewable Energy, Vehicle Technologies Program.

■ REFERENCES

(1) Gasteiger, H. A.; Kocha, S. S.; Sompalli, B.; Wagner, F. T. Activity Benchmarks and Requirements for Pt, Pt-Alloy, and Non-Pt Oxygen Reduction Catalysts for PEMFCs. *Appl. Catal., B* **2005**, *56*, 9−35.

(2) Nilekar, A.; Xu, Y.; Zhang, J.; Vukmirovic, M.; Sasaki, K.; Adzic, R.; Mavrikakis, M. Bimetallic and Ternary Alloys for Improved Oxygen Reduction Catalysis. *Top. Catal.* **2007**, *46*, 276−284.

(3) Zhang, J.; Lima, F. H. B.; Shao, M. H.; Sasaki, K.; Wang, J. X.; Hanson, J.; Adzic, R. R. Platinum Monolayer on Nonnoble Metal−Noble Metal Core−Shell Nanoparticle Electrocatalysts for O_2 Reduction. *J. Phys. Chem. B* **2005**, *109*, 22701−22704.

(4) Stamenkovic, V. R.; Mun, B. S.; Arenz, M.; Mayrhofer, K. J. J.; Lucas, C. A.; Wang, G. F.; Ross, P. N.; Markovic, N. M. Trends in Electrocatalysis on Extended and Nanoscale Pt-Bimetallic Alloy Surfaces. *Nat. Mater.* **2007**, *6*, 241−247.

(5) Stamenkovic, V. R.; Fowler, B.; Mun, B. S.; Wang, G.; Ross, P. N.; Lucas, C. A.; Marković, N. M. Improved Oxygen Reduction Activity on $Pt_3Ni(111)$ via Increased Surface Site Availability. *Science* **2007**, *315*, 493−497.

(6) Stamenkovic, V. R.; Mun, B. S.; Mayrhofer, K. J. J.; Ross, P. N.; Markovic, N. M. Effect of Surface Composition on Electronic Structure, Stability, and Electrocatalytic Properties of Pt-Transition Metal Alloys: Pt-Skin versus Pt-Skeleton Surfaces. *J. Am. Chem. Soc.* **2006**, *128*, 8813−8819.

(7) Xu, Y.; Ruban, A. V.; Mavrikakis, M. Adsorption and Dissociation of O_2 on Pt−Co and Pt−Fe Alloys. *J. Am. Chem. Soc.* **2004**, *126*, 4717−4725.

(8) Norskov, J. K.; Bligaard, T.; Rossmeisl, J.; Christensen, C. H. Towards the Computational Design of Solid Catalysts. *Nat. Chem.* **2009**, *1*, 37−46.

(9) Chen, S.; Ferreira, P. J.; Sheng, W.; Yabuuchi, N.; Allard, L. F.; Shao-Horn, Y. Enhanced Activity for Oxygen Reduction Reaction on "Pt_3Co" Nanoparticles: Direct Evidence of Percolated and Sandwich-Segregation Structures. *J. Am. Chem. Soc.* **2008**, *130*, 13818−13819.

(10) Chen, S.; Sheng, W.; Yabuuchi, N.; Ferreira, P. J.; Allard, L. F.; Shao-Horn, Y. Origin of Oxygen Reduction Reaction Activity on "Pt_3Co" Nanoparticles: Atomically Resolved Chemical Compositions and Structures. *J. Phys. Chem. C* **2009**, *113*, 1109−1125.

(11) Mathias, M. F.; Makharia, R.; Gasteiger, H. A.; Conley, J. J.; Fuller, T. J.; Gittleman, C. J.; Kocha, S. S.; Miller, D. P.; Mittelsteadt, C. K.; Xie, T.; Yan, S. G.; Yu, P. T. Two Fuel Cell Cars In Every Garage? *Electrochem. Soc. Interface* **2005**, *14*, 24−35.

(12) Ball, S. C.; Hudson, S. L.; Theobald, B. R.; Thompsett, D. PtCo, a Durable Catalyst for Automotive PEMFC? *ECS Trans.* **2007**, *11*, 1267−1278.

(13) Wagner, F. T.; Gasteiger, H. A.; Makharia, R.; Neyerlin, K. C.; Thompson, E. L.; Yan, S. G. Catalyst Development Needs and Pathways for Automotive PEM Fuel Cells. *ECS Trans.* **2006**, *3*, 19−29.

(14) Chen, S.; Gasteiger, H. A.; Hayakawa, K.; Tada, T.; Shao-Horn, Y. Platinum-Alloy Cathode Catalyst Degradation in Proton Exchange Membrane Fuel Cells: Nanometer-Scale Compositional and Morphological Changes. *J. Electrochem. Soc.* **2010**, *157*, A82−A97.

(15) Ferreira, P. J.; la O', G. J.; Shao-Horn, Y.; Morgan, D.; Makharia, R.; Kocha, S.; Gasteiger, H. A. Instability of Pt/C Electrocatalysts in Proton Exchange Membrane Fuel Cells - a Mechanistic Investigation. *J. Electrochem. Soc.* **2005**, *152*, A2256−A2271.

(16) Wang, D.; Xin, H. L.; Yu, Y.; Wang, H.; Rus, E.; Muller, D. A.; Abruña, H. D. Pt-Decorated PdCo@Pd/C Core−Shell Nanoparticles with Enhanced Stability and Electrocatalytic Activity for the Oxygen Reduction Reaction. *J. Am. Chem. Soc.* **2010**, *132*, 17664−17666.

(17) Lai, F. J.; Su, W. N.; Sarma, L. S.; Liu, D. G.; Hsieh, C. A.; Lee, J. F.; Hwang, B. J. Chemical Dealloying Mechanism of Bimetallic Pt-Co Nanoparticles and Enhancement of Catalytic Activity toward Oxygen Reduction. *Chemistry* **2010**, *16*, 4602−4611.

(18) Wang, J. X.; Inada, H.; Wu, L.; Zhu, Y.; Choi, Y.; Liu, P.; Zhou, W.-P.; Adzic, R. R. Oxygen Reduction on Well-Defined Core−Shell Nanocatalysts: Particle Size, Facet, and Pt Shell Thickness Effects. *J. Am. Chem. Soc.* **2009**, *131*, 17298−17302.

(19) Dubau, L.; Durst, J.; Maillard, F.; Guétaz, L.; Chatenet, M.; André, J.; Rossinot, E. Further Insights into the Durability of Pt_3Co/C Electrocatalysts: Formation of "Hollow" Pt Nanoparticles Induced by the Kirkendall Effect. *Electrochim. Acta* **2011**, *56*, 10658−10667.
(20) Mazumder, V.; Chi, M.; More, K. L.; Sun, S. Core/Shell Pd/FePt Nanoparticles as an Active and Durable Catalyst for the Oxygen Reduction Reaction. *J. Am. Chem. Soc.* **2010**, *132*, 7848−7849.
(21) Zhou, W.-P.; Sasaki, K.; Su, D.; Zhu, Y.; Wang, J. X.; Adzic, R. R. Gram-Scale-Synthesized Pd_2Co-Supported Pt Monolayer Electrocatalysts for Oxygen Reduction Reaction. *J. Phys. Chem. C* **2010**, *114*, 8950−8957.
(22) Shao-Horn, Y.; Sheng, W. C.; Chen, S.; Ferreira, P. J.; Holby, E. F.; Morgan, D. Instability of Supported Platinum Nanoparticles in Low-Temperature Fuel Cells. *Top. Catal.* **2007**, *46*, 285−305.
(23) Ferreira, P. J.; Shao-Horn, Y. Formation Mechanism of Pt Single-Crystal Nanoparticles in Proton Exchange Membrane Fuel Cells. *Electrochem. Solid-State Lett.* **2007**, *10*, B60−B63.
(24) Holby, E. F.; Sheng, W.; Shao-Horn, Y.; Morgan, D. Pt Nanoparticle Stability in PEM Fuel Cells: Influence of Particle Size Distribution and Crossover Hydrogen. *Energy Environ. Sci.* **2009**, *2*, 865−871.
(25) Xin, H. L.; Mundy, J. A.; Liu, Z.; Cabezas, R.; Hovden, R.; Kourkoutis, L. F.; Zhang, J.; Subramanian, N. P.; Makharia, R.; Wagner, F. T.; Muller, D. A. Atomic-Resolution Spectroscopic Imaging of Ensembles of Nanocatalyst Particles Across the Life of a Fuel Cell. *Nano Lett.* **2011**, Article ASAP, DOI: 10.1021/nl203975u.
(26) Cliff, G.; Lorimer, G. W. The Quantitative Analysis of Thin Specimens. *J. Microsc.* **1975**, *103*, 203−207.
(27) Sheng, W.; Chen, S.; Vescovo, E.; Shao-Horn, Y. Size Influence on the Oxygen Reduction Reaction Activity and Instability of Supported Pt Nanoparticles. *J. Electrochem. Soc.* **2011**, *159*, B1−B8.
(28) Mayrhofer, K. J. J.; Strmcnik, D.; Blizanac, B. B.; Stamenkovic, V.; Arenz, M.; Markovic, N. M. Measurement of Oxygen Reduction Activities via the Rotating Disc Electrode Method: From Pt Model Surfaces to Carbon-Supported High Surface Area Catalysts. *Electrochim. Acta* **2008**, *53*, 3181−3188.
(29) Schlapka, A.; Lischka, M.; Gross, A.; Käsberger, U.; Jakob, P. Surface Strain versus Substrate Interaction in Heteroepitaxial Metal Layers: Pt on Ru(0001). *Phys. Rev. Lett.* **2003**, *91*, 016101−016104.
(30) Jalan, V.; Taylor, E. J. Importance of Interatomic Spacing in Catalytic Reduction of Oxygen in Phosphoric-Acid. *J. Electrochem. Soc.* **1983**, *130*, 2299−2301.
(31) Mukerjee, S.; Srinivasan, S. Enhanced Electrocatalysis of Oxygen Reduction on Platinum Alloys in Proton-Exchange Membrane Fuel-Cells. *J. Electroanal. Chem.* **1993**, *357*, 201−224.
(32) Mukerjee, S.; Srinivasan, S.; Soriaga, M. P.; Mcbreen, J. Effect of Preparation Conditions of Pt Alloys on Their Electronic, Structural, and Electrocatalytic Activities for Oxygen Reduction-Xrd, Xas, and Electrochemical Studies. *J. Phys. Chem.* **1995**, *99*, 4577−4589.
(33) Toda, T.; Igarashi, H.; Uchida, H.; Watanabe, M. Enhancement of the Electroreduction of Oxygen on Pt Alloys with Fe, Ni, and Co. *J. Electrochem. Soc.* **1999**, *146*, 3750−3756.
(34) Mukerjee, S.; Srinivasan, S.; Soriaga, M. P.; Mcbreen, J. Role of Structural and Electronic-Properties of Pt and Pt Alloys on Electrocatalysis of Oxygen Reduction - An in-Situ Xanes and Exafs Investigation. *J. Electrochem. Soc.* **1995**, *142*, 1409−1422.
(35) Adzic, R. R.; Zhang, J.; Sasaki, K.; Vukmirovic, M. B.; Shao, M.; Wang, J. X.; Nilekar, A. U.; Mavrikakis, M.; Valerio, J. A.; Uribe, F. Platinum Monolayer Fuel Cell Electrocatalysts. *Top. Catal.* **2007**, *46*, 249−262.
(36) Erlebacher, J. An Atomistic Description of Dealloying - Porosity Evolution, The Critical Potential, And Rate-Limiting Behavior. *J. Electrochem. Soc.* **2004**, *151*, C614−C626.
(37) Erlebacher, J.; Aziz, M. J.; Karma, A.; Dimitrov, N.; Sieradzki, K. Evolution of Nanoporosity in Dealloying. *Nature* **2001**, *410*, 450−453.